EARTHQUAKE ENGINEERING AND STRUCTURAL DYNAMICS
Earthquake Engng Struct. Dyn. 2000; **29**: 441–460

A method for coupled arch dam-foundation-reservoir seismic behaviour analysis

R. J. Câmara*

Laboratório Nacional de Engenharia Civil, Portugal

SUMMARY

This paper presents a method for coupled arch dam–foundation–reservoir seismic behaviour analysis. The dam is discretized by finite elements (FE) and the foundation and reservoir are discretized by boundary elements (BE). The opening of contraction joints and the spatial variability of the seismic action is taken into account. The study of Pacoima dam by this method is also presented. The computed results show that no cracks were to be expected due to the vibrations induced during the Feb. 9, 1971 San Fernando earthquake.
Copyright © 2000 John Wiley & Sons, Ltd.

KEY WORDS: seismic response; arch dams; non-linear; contraction joints; interaction; hybrid method

1. INTRODUCTION

The linear elastic behaviour of arch dams during low-intensity earthquakes is a reasonable approximation. The infinite dimension of the foundation originates radiation damping. In the present work, the dam's foundation is analysed by a boundary element method in the frequency domain. The canyon is assumed 3D, with an uniform cross-section. In the same way, the reservoir is assumed infinite, with an uniform cross-section. It is also analysed by a boundary element method, in the frequency domain. The dam is assumed to be a thin shell and is discretized by triangular elements. So, both the dam and reservoir only need the dam's middle surface discretization, and the foundation is defined by the insertion. The earthquake is characterised by a power density spectrum of accelerations on a half-space point. The spatial variability is taken into account by a boundary element method analysis of a SH wave model with an arbitrary spatial incidence on the canyon.

The behaviour of arch dams during high-intensity earthquakes may be idealized as non-linear. In the present model, the non-linear behaviour is assumed to be due to the no-tension contraction joints. The earthquake is assumed being defined by an acceleration time history. A stress transfer

* Correspondence to: R. J. Câmara, Departamento de Barragens, Laboratório Nacional de Engenharia Civil, Av. Do Brasil 101, 1799 Lisboa Codex, Portugal.

Received 4 June 1998
Revised 29 June 1999
Accepted 14 September 1999

Copyright © 2000 John Wiley & Sons, Ltd.

technique is used, where the unbalanced forces in the time domain are transformed to the frequency domain, allowing a frequency analysis of the system, going afterwards to the time domain and then performing a new evaluation of the unbalanced forces. The scheme is repeated until convergence is attained. The spatial variability of the earthquake is also considered in the frequency domain by the adopted wave model.

In order to take into account the opening of contraction joints, Dowling and Hall [1] used a step by step time scheme, but assumed uniform earthquakes. The influence of the spatial variability of the earthquakes was also taken into account by Mojtahedi and Fenves [2], but assumed rigid water and massless foundation. The present method takes into account all of these aspects.

2. FOUNDATION ANALYSIS BY THE BOUNDARY ELEMENT METHOD

The canyon cross-section was assumed uniform. Therefore, according to Zhang and Chopra [3], it is possible to use the transform G_{ij} towards the co-ordinate x_1 (along the canyon axis), of the displacement's fundamental solution G_{ij}^* (component i), due to a point load (along x_j) applied on the full space,

$$G_{ij}(\mathbf{x}_0, \mathbf{x}_{0s}, k) = \int_{-\infty}^{\infty} G_{ij}^*(\mathbf{x}, \mathbf{x}_{0s}) \exp(-\mathrm{j}kx_1)\, \mathrm{d}x_1 \tag{1}$$

for a receiver at $\mathbf{x} = (x_1, x_2, x_3)$ and a source at $\mathbf{x}_{0s} = (0, x_{02}, x_{03})$, where k is the wave number and $\mathbf{x}_{0s} = (x_2, x_3)$.

The transform $\overset{n}{F}$ of the stresses $\overset{n}{F}{}^*$ due to G^*, at a face of unitary normal $\mathbf{n}$,

$$\overset{n}{F}_{ij}(\mathbf{x}_0, \mathbf{x}_{0s}, k) = \int_{-\infty}^{\infty} \overset{n}{F}{}_{ij}^*(\mathbf{x}, \mathbf{x}_{0s}) \exp(-\mathrm{j}kx_1)\, \mathrm{d}x_1 \tag{2}$$

may be directly computed from $G_{ij}(\mathbf{x}_0, \mathbf{x}_{0s}, k)$ for the elastic constants E and v.

Let be $\{\bar{U}(\mathbf{x}_0, k)\}$ and $\{\bar{t}(\mathbf{x}_0, k)\}$ the Fourier transforms along x_1 of the displacements and stresses at the boundary surface $\{U(\mathbf{x})\}$ e $\{t(\mathbf{x})\}$. Then

$$\{U(\mathbf{x})\} = \int_{-\infty}^{\infty} \{\bar{U}(\mathbf{x}_0, k)\} \exp(-\mathrm{j}kx_1)\, \mathrm{d}k \tag{3}$$

and

$$\{t(\mathbf{x})\} = \int_{-\infty}^{\infty} \{\bar{t}(\mathbf{x}_0, k)\} \exp(-\mathrm{j}kx_1)\, \mathrm{d}k \tag{4}$$

The transformed representation theorem is obtained replacing Equations (3) and (4) in the 3D representation principle, changing the order of integration and taking into account Equations (1)

Copyright © 2000 John Wiley & Sons, Ltd

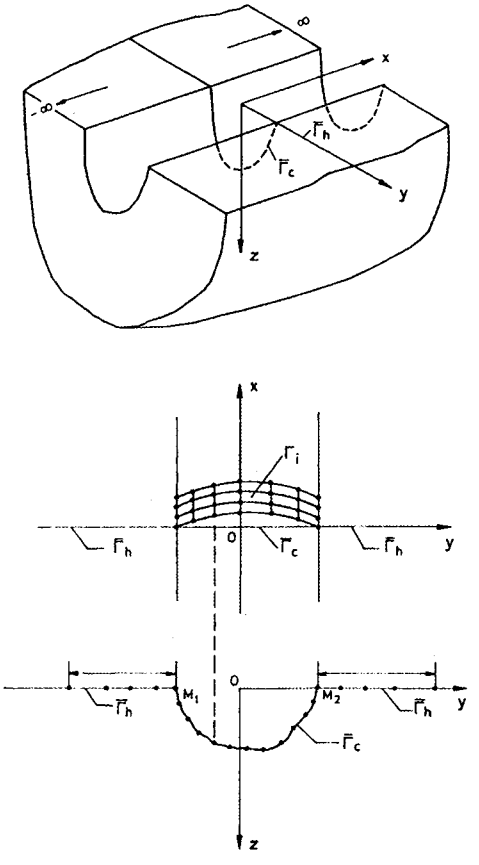

Figure 1. Foundation model.

and (2),

$$[C(\mathbf{x}_{0s})]\,\{\bar{U}(\mathbf{x}_{0s}, k)\} + \int_{\bar{\Gamma}_c \cap \bar{\Gamma}_h} [\overset{n}{F}(\mathbf{x}_0, \mathbf{x}_{0s}, k)]^T (\bar{U}(\mathbf{x}_0, k)\}\, d\Gamma$$

$$= \int_{\bar{\Gamma}_c \cap \bar{\Gamma}_h} [G(\mathbf{x}_0, \mathbf{x}_{0s}, k)]^T \{\bar{t}(\mathbf{x}_0, k)\}\, d\Gamma \tag{5}$$

where $\bar{\Gamma}_c e \bar{\Gamma}_h$ are, respectively, Figure 1 (according to Ref. [3]), the boundary lines of the canyon and half-space cross-section and $[C(\mathbf{x}_{0s})]$ is the matrix that corrects the values of displacements at a boundary point $\mathbf{x}_{0s}$, when the line has different right and left derivatives. For equal derivatives the matrix is diagonal with diagonal values equal to 0.5.

Based upon the representation theorem, the following discretized equations are obtained:

$$[A(k)]\,\{\bar{U}\} = [B(k)]\,\{T\}$$

Copyright © 2000 John Wiley & Sons, Ltd

where $\{\bar{U}\}$ are the transformed nodal displacements at $\bar{\Gamma}_c \cup \bar{\Gamma}_h$, $\{T\}$ are the transformed nodal stresses at the interface between the dam and foundation Γ_i and

$$[A(k)] = \begin{pmatrix} [C(\mathbf{x}_1)] & & & \\ & \cdot & & \\ & & \cdot & \\ & & & [C(\mathbf{x}_{M_n})] \end{pmatrix} + \begin{pmatrix} [\tilde{A}(\mathbf{x}_1, k)] \\ \cdot \\ \cdot \\ [\tilde{A}(\mathbf{x}_{M_n}, k)] \end{pmatrix}$$

$$[B(k)] = \begin{pmatrix} [\tilde{B}(\mathbf{x}_1, k)] \\ \cdot \\ \cdot \\ [\tilde{B}(\mathbf{x}_{M_n}, k)] \end{pmatrix}$$

$$[\tilde{A}(\mathbf{x}_{0s}, k)] = \frac{1}{2} \sum_{j=1}^{M} l_j \int_{-1}^{1} [\overset{n}{F}(\tau, \bar{x}_{0s}, k)]_i^{\mathrm{T}} [N(\tau)] \, \mathrm{d}\tau$$

$$[\tilde{B}(\mathbf{x}_{0s}, k)] = \frac{1}{2} \sum_{j=M_1}^{M_2} l_j \int_{-1}^{1} [G(\tau, \bar{x}_{0s}, k)]_j^{\mathrm{T}} [\bar{H}(\tau, k)]_j \, \mathrm{d}\tau$$

M_n is the number of nodal points and M the number of elements at $\bar{\Gamma}_c \cup \bar{\Gamma}_h$. $M_1 \ldots M_2$ are the elements at $\bar{\Gamma}_c$. l_j is the length of the element j. The relationship between the transformed fields of displacements $\{\bar{U}(\mathbf{x}_0, k)\}_j$ and stresses $\{\bar{t}(\mathbf{x}_0, k)\}_j$ at element j, with the transformed nodal displacements $\{\bar{U}\}_j$ and nodal stresses $\{T\}_j$ (nodal points of surface elements at Γ_i, intercepted by the line $\mathbf{x} = \mathbf{x}_0$; For the thin shell elements quadrilaterals with two sides parallel to x_1 axis are used) are assumed:

$$\{\bar{t}(\mathbf{x}_0, k)\}_j = [\bar{H}(\mathbf{x}_0, k)]_j \{T\}_j$$

$$\{\bar{U}(\mathbf{x}_0, k)\}_j = [N] \{\bar{U}\}_j$$

solving for transformed displacements:

$$\{\bar{U}\} = [A(k)]^{-1} [B(k)] \{T\}$$

Numerical evaluation of

$$\{U(\mathbf{x})\} = \int_{-\infty}^{\infty} \{\bar{U}(\mathbf{x}_0, k)\} \, \mathrm{e}^{-\mathrm{j}kx} \, \mathrm{d}k, \quad \mathbf{x} \in \Gamma_h \cup \Gamma_c$$

Copyright © 2000 John Wiley & Sons, Ltd

is

$$\{U(\mathbf{x})\} = \sum_q w_q \{\bar{U}(\mathbf{x}_0, k_q)\} \, \mathrm{e}^{-\mathrm{j}k_q x}$$

where w_q are weighting coefficients. The displacement vector at nodal point j of Γ_i, with co-ordinates $\mathbf{x}_j = (x_j, y_j, z_j)$ is expressed by

$$\{\bar{r}_j\} = \sum_q w_q \{\bar{U}(\mathbf{x}_{0j}, k_q)\} \mathrm{e}^{-\mathrm{j}k_q x_j}$$

where

$$\{\bar{U}(\mathbf{x}_{0j}, k_q)\} = \{\bar{U}_j\}$$

In the present case the interpolation between two points at $\bar{\Gamma}_c$ is not necessary, because the points at Γ_i are directed along the x_1-axis, Figure 1. Taking into account that the nodal displacements are combinations of the nodal stresses $\{T\}$, we have

$$\{\bar{U}(\mathbf{x}_{0j}, k_q)\} = [E(\mathbf{x}_{0j}, k_q)] \{T\}$$

Therefore, the displacements in the frequency domain, $\{\bar{r}_j\}$, at nodal point j are

$$\{\bar{r}_j\} = [\tilde{f}_j] \{T\}$$

with

$$[\tilde{f}_j] = \sum_q w_q [E(\mathbf{x}_{0j}, k_q)] \mathrm{e}^{-\mathrm{j}k_q x_j}$$

assembling for the M_i nodal points at Γ_i

$$\{\bar{r}\} = [f]\{T\}$$

being $[f]$ a square matrix of rank $3M_i$

assuming the stresses obtained by linear interpolation

$$\{t(\mathbf{x})\} = [h(\mathbf{x})] \{T\}$$

related to nodal forces $\{\bar{R}\}$ by

$$\{\bar{R}\} = [\phi] \{T\}$$

Copyright © 2000 John Wiley & Sons, Ltd

with

$$[\phi] = \int_{\Gamma_i} [h(\mathbf{x})]^{\mathrm{T}} [h(\mathbf{x})] \, \mathrm{d}\Gamma$$

then

$$\{\bar{R}(w)\} = [\phi][f(w)]^{-1} \{\bar{r}(w)\}$$

and the $3M_i \times 3M_i$ impedance matrix is obtained:

$$[\hat{S}(w)] = [\phi][f(w)]^{-1}$$

or by symmetrization we obtain the impedance matrix for 3D displacements ('g' refers to ground, and 'b' to nodes at structure–rock interface):

$$[S^{\mathrm{g}}_{\mathrm{bb}}(w)]^{3\mathrm{D}} = \tfrac{1}{2}([\hat{S}(w)] + [\hat{S}(w)]^{\mathrm{T}})$$

The displacements at each pair of points (one upstream $U_m^{\mathrm{U}(L)}$, one downstream $U_m^{\mathrm{D}(L)}$, L being the distance between them) are related to the medium displacements U_m^{S} and to rotations θ_m^{S} (S — from shell) by

$$U_m^{\mathrm{U}(L)} = U_m^{\mathrm{S}} + (-1)^m \frac{L}{2} \theta_n^{\mathrm{S}}$$

$$U_m^{\mathrm{D}(L)} = U_m^{\mathrm{S}} - (-1)^m \frac{L}{2} \theta_n^{\mathrm{S}}$$

$$(m = 2, 3;\ n = 3, 2)$$

$$U_1^{\mathrm{U}(L)} = U_1^{\mathrm{D}(L)} = U_1^{\mathrm{S}}$$

where the downstream–upstream direction is directed along the x_1-axis, and the downwards direction along the x_3-axis. The discretization of Γ_i, Figure 1, is done by symmetrical points to the shell insertion, and directed along the x_1-axis. In matrix notation

$$\{\bar{r}\} = [A]\{r\}^{\mathrm{S}}$$

so that

$$[S^{\mathrm{g}}_{\mathrm{bb}}(\omega)] = [A]^{\mathrm{T}} [S^{\mathrm{g}}_{\mathrm{bb}}(\omega)]^{3\mathrm{D}} [A]$$

According to Ref. [3] the solution of the scattering wave problems is based on Equation (5) replacing $\{\bar{t}(\mathbf{x}_0)\}$ by $-\{t^n_{\mathrm{ff}}(\mathbf{x}_0)\}$, which represents the fictitious stresses along the cross-section of the canyon, due to the 'free-field' (indice 'ff') wave stresses at the half-space. In this expression $\{\bar{U}\}$ are the scattering displacements.

Copyright © 2000 John Wiley & Sons, Ltd

3. RESERVOIR ANALYSIS BY THE BOUNDARY ELEMENT METHOD

The reservoir cross-section was assumed uniform. The hydrodynamic pressure of reservoir's fundamental solution satisfies rigid bottom boundary conditions and zero hydrodynamic pressure at free surface. The fundamental solution P^*, due to a source $\delta(\boldsymbol{\xi})$ (where δ is the distribution of Dirac) in the reservoir, may be computed from the modes of vibration $\psi_n(x_1, x_2)$ (with natural frequencies Λ_n; C_0 is the sound wave propagation velocity) of a cross-section where x_3 is the reservoir axis. According to Câmara [4]:

$$P^*(\mathbf{x}, \boldsymbol{\xi}) = \sum_n \frac{\psi_n(x_1, x_2)\psi_n(\xi_1, \xi_2)}{2\chi_n} \exp(-|\xi_3 - x_3|\chi_n) \tag{6}$$

where

$$\chi_n^2 = \frac{\Lambda_n^2 - \omega^2}{C_0^2}$$

with the source at $\boldsymbol{\xi}$ and the receiver at $\mathbf{x}$. ω is the frequency of the harmonic vibrations. The vibration modes problem are expressed by

$$\sum_{m=1}^{2} \frac{\partial^2 \psi_n(x_1, x_2)}{\partial x_m^2} = -\frac{\Lambda_n^2}{C_0^2} \psi_n(x_1, x_2) \tag{7}$$

satisfying the boundary conditions

$$\psi_n(x_1, x_2) = 0 \quad \text{at the free surface}$$

and

$$\sum_{m=1}^{2} \frac{\partial \psi_n(x_1, x_2)}{\partial x_m} \lambda_m(x_1, x_2) = 0 \quad \text{at the bottom}$$

$\lambda_m(x_1, x_2)$ is the m component of the unitary normal to the boundary line of the cross-section at (x_1, x_2). The orthogonality conditions are

$$\int_A \psi_m(x_1, x_2)\psi_n(x_1, x_2)\, \mathrm{d}x_1\, \mathrm{d}x_2 = \delta_{mn}$$

Let P^* and P be, respectively, the fundamental solution and the solution of the pressure wave equation, for harmonic vibrations, satisfying at the free surface $P = 0$ and where the normal pressure gradient is fixed at the structure–fluid interface Ω. Taking into account the conventions

Copyright © 2000 John Wiley & Sons, Ltd

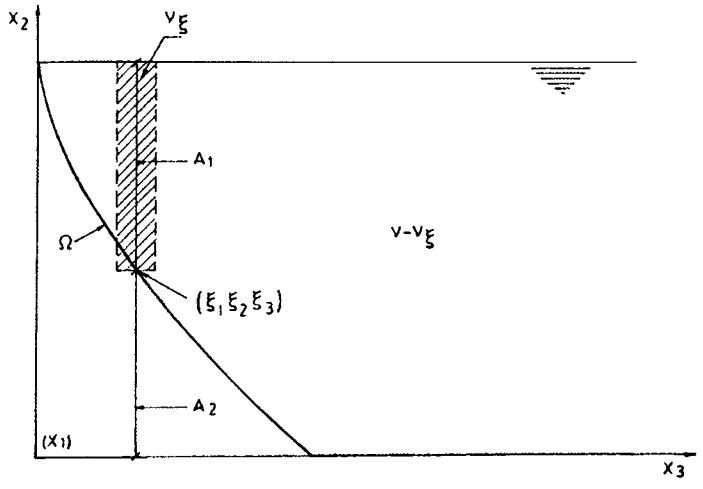

Figure 2. Reservoir's conventions.

shown in Figure 2, we obtain

$$\int_{V-V_\xi}\left(\sum_{m=1}^{3}\frac{\partial^2 P^*}{\partial x_m^2}+k^2P^*\right)P\,\mathrm{d}v+\int_{V_\xi}\left(\sum_{m=1}^{3}\frac{\partial^2 P^*}{\partial x_m^2}+k^2P^*\right)P\,\mathrm{d}v$$

$$=-\int_\Omega P^*\frac{\partial P}{\partial \lambda}\,\mathrm{d}s+\int_\Omega \frac{\partial P^*}{\partial \lambda}P\,\mathrm{d}s$$

The summation in $V-V_\xi$ is equal to zero because

$$\sum_{m=1}^{3}\frac{\partial^2 P^*}{\partial x_m^2}+k^2P^*=0 \quad \text{if } x_3\neq\xi_3$$

The summation in V_ξ, when the limit of V_ξ, is equal to zero becomes

$$\int_{V_\xi}\left(\sum_{m=1}^{3}\frac{\partial^2 P^*}{\partial x_m^2}+k^2P^*\right)P\,\mathrm{d}v$$

$$=-\sum_n\int_{A_1}P(x_1,x_2,\xi_3)\,\psi_n(x_1,x_2)\psi_n(\xi_1,\xi_2)\;\mathrm{d}x_1\,\mathrm{d}x_2$$

On the other side,

$$\sum_n\int_{A_1}P(x_1,x_2,\xi_3)\,\psi_n(x_1,x_2)\psi_n(\xi_1,\xi_2)\,\mathrm{d}x_1\,\mathrm{d}x_2$$

Copyright © 2000 John Wiley & Sons, Ltd

$$
\begin{aligned}
&- \sum_n \int_{A_1} P(x_1, x_2, x_3(x_1, x_2)) \frac{\psi_n(x_1, x_2)\psi_n(\xi_1, \xi_2)}{2} \mathrm{e}^{-(\xi_3 - x_3(x_1, x_2))\chi_n} \, \mathrm{d}x_1 \, \mathrm{d}x_2 \\
&+ \sum_n \int_{A_2} P(x_1, x_2, x_3(x_1, x_2)) \frac{\psi_n(x_1, x_2)\psi_n(\xi_1, \xi_2)}{2} \mathrm{e}^{-(x_3(x_1, x_2) - \xi_3)\chi_n} \, \mathrm{d}x_1 \, \mathrm{d}x_2 \\
&= \sum_n \int_{A_1 + A_2} [g(x_1, x_2)] \psi_n(x_1, x_2)\psi_n(\xi_1, \xi_2) \, \mathrm{d}x_1 \, \mathrm{d}x_2 = g(\xi_1, \xi_2)
\end{aligned}
$$

where

$$
g(x_1, x_2) = P(x_1, x_2, \xi_3) - \tfrac{1}{2} P(x_1, x_2, x_3(x_1, x_2)) \mathrm{e}^{-(\xi_3 - x_3(x_1, x_2))\chi_n} \quad \text{if } x \in A_1
$$

$$
g(x_1, x_2) = \frac{P(x_1, x_2, x_3(x_1, x_2))}{2} \mathrm{e}^{-(x_3(x_1, x_2) - \xi_3)\chi_n} \quad \text{if } x \in A_2
$$

On the contact line between A_1 and A_2, $x_3(x_1, x_2) = \xi_3$, so $g(x_1, x_2) = \frac{1}{2} P(x_1, x_2, \xi_3)$. If the point is on the surface $g(\xi_1, \xi_2) = \frac{1}{2} P(\xi_1, \xi_2, \xi_3)$.

So taking into account

$$
\begin{aligned}
&\sum_n \int_{A_1} P(x_1, x_2, \xi_3)\psi_n(x_1, x_2)\psi_n(\xi_1, \xi_2) \, \mathrm{d}x_1 \, \mathrm{d}x_2 \\
&\quad - \sum_n \int_{A_1} P(x_1, x_2, x_3(x_1, x_2)) \frac{\psi_n(x_1, x_2)\, \psi_n(\xi_1, \xi_2)}{2} \mathrm{e}^{-(\xi_3 - x_3\,(x_1, x_2))\chi_n} \, \mathrm{d}x_1 \, \mathrm{d}x_2 \\
&\quad + \sum_n \int_{A_2} P(x_1, x_2, x_3(x_1, x_2)) \frac{\psi_n(x_1, x_2)\psi_n(\xi_1, \xi_2)}{2} \mathrm{e}^{-(x_3(x_1, x_2) - \xi_3)\chi_n} \, \mathrm{d}x_1 \, \mathrm{d}x_2 \\
&= \frac{1}{2} P(\xi_1, \xi_2, \xi_3)
\end{aligned}
$$

we obtain the representation theorem,

$$
\begin{aligned}
\frac{1}{2} P(\xi_1, \xi_2, \xi_3) = &- \sum_n \int_\Omega \sum_{m=1}^{2} P(x_1, x_2, x_3) \frac{\partial \psi_n(x_1, x_2)}{\partial x_m} \frac{\psi_n(\xi_1, \xi_2)}{2\chi_n} \mathrm{e}^{-|\xi_3 - x_3|\chi_n} \lambda_m \, \mathrm{d}s \\
&+ \sum_n \int_\Omega \frac{\partial P(x_1, x_2, x_3)}{\partial \lambda} \frac{\psi_n(x_1, x_2)\psi_n(\xi_1, \xi_2)}{2\chi_n} \mathrm{e}^{-|\xi_3 - x_3|\chi_n} \, \mathrm{d}s
\end{aligned}
$$

This result is by no means trivial because the summation in m is from 1 to 2 and not 3. In order to discretize the motion equations, the vibration modes of the reservoir cross-section are numerically computed from a finite element discretization of the cross-section. Triangular elements with three nodes are used, the pressures being obtained by linear interpolation with area

Copyright © 2000 John Wiley & Sons, Ltd

shape functions L_i. The vibration modes ψ'_{ni} satisfy the orthogonality conditions

$$\psi'_{ni}\bar{K}_{ij}\psi'_{mj} = \delta_{mn}\Lambda_n^2$$
$$\psi'_{ni}\bar{M}_{ij}\psi'_{mj} = \delta_{mn} \quad (i, j = 1, 2, \ldots) \quad (m, n = 1, 2, \ldots)$$

Here $\bar{K}$ and $\bar{M}$ are respectively, the finite elements 'stiffness' and 'mass' matrices of the discretized 2-D cross-section compatible with the boundary discretization of the shell–fluid interface. Taking into account the normalization used for the fundamental solution we obtain

$$\psi_{ni} = \frac{\psi'_{ni}}{C_0}$$
$$\psi_m(x_1, x_2) = \sum_{i=1}^{3} L_i\psi_{mi}$$

The discretized global motion equations, obtained from the representation theorem are expressed by

$$\frac{1}{2}P_i = G_{ij}\left(\frac{\partial P}{\partial \lambda}\right)_j - H'_{ij}P_j$$

where

$$G_{ij} = \sum_k \int_{\Omega_k} \sum_l \sum_n L_j L_l \frac{\psi_{nl}\psi_{ni}}{2\chi_n} \mathrm{e}^{-|\xi_3^i - x_3|\chi_n} \, \mathrm{d}s$$
$$H'_{ij} = \sum_k \int_{\Omega_k} \sum_l \sum_n \sum_{m=1}^{2} L_j \frac{b_{lm}}{\phi} \frac{\psi_{nl}\psi_{ni}}{2\chi_n} \mathrm{e}^{-|\xi_3^i - x_3|\chi_n} \lambda_m \, \mathrm{d}s$$

($k = 1, \ldots, n^\circ$ of elements), ($n = 1, \ldots, n^\circ$ of vibration modes), ($i, j = 1, \ldots, n^\circ$ of nodal points), Ω_k is the area of element k and $(\xi_1^i, \xi_2^i, \xi_3^i)$ are the co-ordinates of node i. $b_{lm}/\phi = \partial L_l/\partial x_m$. The summation in Ω_k follows the scheme: index 1 takes only the nodal points of Ω_k; the contribution of each vibration mode n is added being the value of the summations assembled at the (i, j) position of the matrixes H'_{ij} and G_{ij}. In matrix notation

$$[G]\left\{\frac{\partial P}{\partial \lambda}\right\} = [H]\{P\} \tag{8}$$

Taking into account that

$$\left\{\frac{\partial P}{\partial \lambda}\right\} = \rho_w\{\ddot{U}_\lambda\} = [A]\{\ddot{U}\}_{\text{shell}}$$

where ρ_w is the mass per unit volume of water, $\{\ddot{U}_\lambda\}$ are the accelerations at nodal points of the shell, directed along the unit vectors normal to the shell–fluid interface and pointing the exterior

Copyright © 2000 John Wiley & Sons, Ltd

of the reservoir, and $\{\ddot{U}\}$ are the accelerations of nodal points of the shell, each with three components. The pressures $\{P\}$ correspond to forces $\{F\}_{\text{shell}}$ applied on the shell

$$[B]\{P\} = \{F\}_{\text{shell}}$$

Solving (8) for $\{P\}$

$$\{P\} = [H]^{-1}[G]\left\{\frac{\partial P}{\partial \lambda}\right\} = [H]^{-1}[G][A]\{\ddot{U}\}$$

so that

$$\{F\}_{\text{shell}} = [S(\omega)]\{U\}_{\text{shell}}$$

where the impedance matrix is given by

$$[S(\omega)] = -\omega^2[B][H(\omega)]^{-1}[G(\omega)][A]$$

4. COUPLED ARCH DAM–FOUNDATION–RESERVOIR ANALYSIS BY THE HYBRID FREQUENCY–TIME METHOD

In order to solve the motion equations of the coupled arch dam–foundation–reservoir, taking into account no tension contraction joints, the hybrid frequency–time method is used, according to Wolf [5]. This method is based on the following scheme:

(1) the FFT (Fast Fourier Transform) of the static forces (Dead Weight and Hydrostatic Pressure; $\{F_s(t)\} = H(t)\{F_s\}$) and of the 'free-field' displacements, $U_b^g(t)$ ('g' denotes ground, the degree of freedom of the interface dam–foundation are referred by 'b' while the others are referred by 's'. $H(t)$ is the Heaviside function), are computed:

$$\{F_s(t)\} \to \{F_s(\omega)\}$$
$$\{U_b^g(t)\} \to \{U_b^g(\omega)\}$$

(2) the impedance matrix $[S_0]$ is evaluated, where $[T] = [K] - \omega^2[M]$ ($[K]$ is the stiffness matrix, $[M]$ the mass matrix of the structure and ω the frequency of harmonic vibrations),

$$[S_0(\omega)] = \begin{bmatrix} [T_{ss}(\omega)] & [T_{sb}(\omega)] \\ [T_{bs}(\omega)] & [T_{bb}(\omega)] + [S_{bb}^g(\omega)] \end{bmatrix}$$

at the discrete frequencies ω_k, until the Nyquist frequency. The discrete frequencies are

$$\omega_k = \frac{2\pi k}{T}, \quad k = 0, \ldots, N/2$$

Copyright © 2000 John Wiley & Sons, Ltd

with $T = N\Delta T$ (T is the duration of the periodic time history of accelerations. It is assumed to be the summation of N time intervals of duration ΔT). The impedance matrix of the reservoir, relating the forces applied by the reservoir on the structure with normal accelerations of the upstream face, is then added to the structure impedance matrix.

(3) the vector of 'real forces', $\{R\}$, applied on the structure is evaluated at the N discrete frequencies,

$$\{R(\omega)\} = \begin{Bmatrix} \{F_s(\omega)\} \\ [S_{bb}^g(\omega)]\{U_b^g(\omega)\} \end{Bmatrix}$$

The discrete Fourier pair transform is

$$X_k = \frac{1}{N}\sum_{r=0}^{N-1} x_r \exp(-j2\pi kr/N) \quad (k = 0, \ldots, N-1)$$

and

$$x_r = \sum_{k=0}^{N-1} X_k \exp(j2\pi kr/N) \quad (r = 0, \ldots, N-1)$$

so

$$X_m = X_{N-m}^* \quad (m = 0, \ldots, N-1)$$

only being necessary the knowledge of X_m until $N/2$. Here $(*)$ indicates the complex conjugate. In order for the time series x_r to be real, it is necessary that $\mathrm{Imag}(X_0) = 0$ and that $\mathrm{Imag}(X_{N/2}) = 0$.

(4) the inverse of the impedance matrix, $[S_0]$, is evaluated at the $N/2$ discrete frequencies,

$$[S_0(\omega)] \to [S_0(\omega)]^{-1}$$

Then the following iterations (j) are done:

(1) the time domain pseudo-forces $\{P_0\}$ are computed,

$$\{P_0^j(t)\} = -\int_S [B]^T \{\sigma_0\}\, dS$$

$$(j = 0; \{P_0^j(t)\} = \{0\})$$

being the integrals evaluated over the joint surfaces and $\{\sigma_0\}$ being the stresses at the open points of the joints (detected by the existence of a normal tension), and $[B]$ the operator relating nodal displacements with strains (in this case the difference between the displacements of two joint faces at the given point).

Copyright © 2000 John Wiley & Sons, Ltd

(2) the unbalanced forces $\{Q\}$ are applied,

$$\{Q^j(t)\} = -\{P_0^j(t)\}$$

(3) after being transformed to the frequency domain,

$$\{Q^j(t)\} \rightarrow \{Q^j(\omega)\}$$

(4) After solving the system of equations for displacements at the $N/2$ discrete frequencies

$$\{U^j(\omega)\} = [S_0(\omega)]^{-1}(\{R(\omega)\} + \{Q^j(\omega)\})$$

(5) the displacements are transformed from frequency domain to time domain, and then return to step (1) in order to evaluate the pseudo-forces, until the scheme converges (the criterion consists in limiting the relative error of unbalanced forces in time domain),

$$\{U^j(\omega)\} \rightarrow \{U^j(t)\}$$

The degrees of freedom at the joints of the coupled system are the mean displacements and rotations and the difference of displacements and rotations between the nodes at the two joint faces. They relate the mean displacements, and so the mean normal accelerations to the shell surface to the hydrodynamic pressures of the reservoir.

A segmenting procedure was adopted, with transition zones at the end of each time segment. The decay filter used in time domain for unbalanced forces was according to Wolf [5]

$$f(t) = 2\left(\frac{t - t_0}{t_1 - t_0}\right)^3 - 3\left(\frac{t - t_0}{t_1 - t_0}\right)^2 + 1$$

t_0 and t_1 are, respectively, the beginning and the end of the transition zone. When convergence was reached in a time step, no change of unbalanced forces up to this step takes place in next iterations. In spite of this procedure, instability was noticed due to high-frequency peak of accelerations during joint closure. So, in order to avoid the causes of instability, a low-pass filter was used in the frequency domain. The criteria of convergence used in the computer scheme assumes that the relative error of the norm of unbalanced forces and moments are both less than 5×10^{-4}.

It was assumed that the stresses at the joint face are

$$\sigma_i = K_i \sum_{j=1}^{2} \sum_{n=1}^{3} (N_{ijn}\Delta U_{jn} + N'_{ijn}\Delta\theta_{jn}) \quad \text{if the normal stress } \sigma_3 \text{ is negative}$$

$$\sigma_i = 0 \quad \text{if the normal stress } \sigma_3 \text{ is positive (tension)}$$

$$(i = 1, 2, 3), \quad K_3 = E/e, \quad K_1 = K_2 = G/e$$

Copyright © 2000 John Wiley & Sons, Ltd

ΔU and $\Delta\theta$ are, respectively, difference of displacements and rotations between pairs of nodal points, each on its side of the joint surface. 'e' is the joint thickness. N_{ijn} and N'_{ijn} are shape functions compatible with thin shell elements based on Hermite polynomials. The joint stiffness was computed by numerical integration (4×6 Gauss points per joint element).

5. EXAMPLE

The seismic behaviour of Pacoima arch dam was analysed by the present method. The dam's response was studied under 5 s of the S75W component of Feb. 9, 1971 San Fernando earthquake [6], recorded near the left abutment of the dam. The dam was analysed in the four following hypotheses:

For hypothesis I, the assumed static actions are the Dead Weight and Water at crest level and for hypothesis II, dead weight and water at $\frac{1}{3}$ of dam's height. Both cases assumed the dam with contraction joints and take as input a time history of accelerations. Considering as static actions dead weight and water at $\frac{1}{3}$ of dam's height, hypothesis III assumes the input as a time history of accelerations and hypothesis IV assumes the input stochastic as a density power spectrum of accelerations. Both III and IV assumed the dam without contraction joints.

All four hypotheses assumed an input of horizontal accelerations at a point on the half-space and distributed along the canyon by a SH wave model with vertically incidence, being the displacements in downstream–upstream direction.

The concrete and rock mass were assumed [2] with an elastic behaviour, characterized by a Young's Modulus of 24 GPa and a Poisson's ratio of 0.2. The unit mass was assumed homogeneous with 2400 Kg/m^3. The hysteretic damping of concrete was assumed 2×0.1 and the hysteretic damping of rock mass was assumed with half the value for concrete. No damping was used in the joints. The normal and the tangential stiffness of contraction joints were assumed 240 and 100 GPa/m, respectively.

The adopted structure and action models are both presented in Figures 3 and 4. The dam is not symmetric due to the left abutment. The peak tensile stresses for different hypotheses are

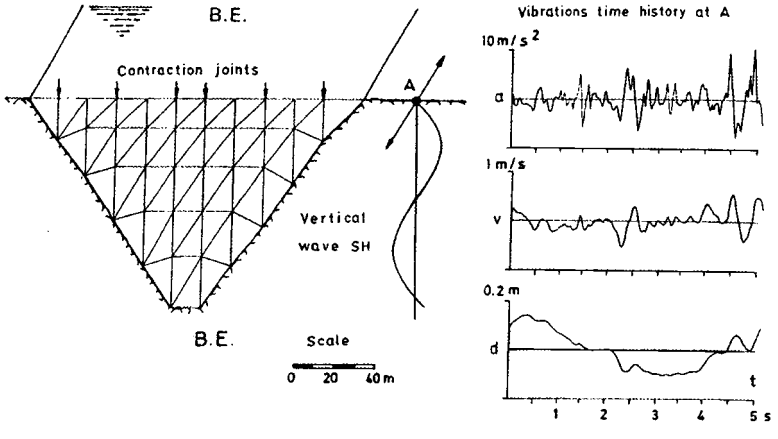

Figure 3. Structure and actions model.

Copyright © 2000 John Wiley & Sons, Ltd

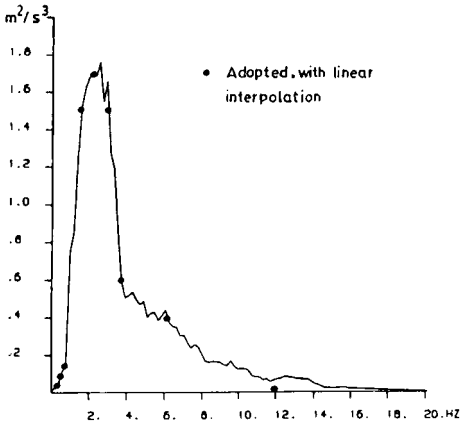

Figure 4. Density power spectrum of accelerations.

presented in Figures 5 and 6. The peak accelerations at dam's body and the joints motion for hypothesis II are presented in Figure 7 (the analysed point is located at crest central cantilever).

For the non-linear analysis a time discretization of 256 time steps (of 0.02 s) was assumed, which was divided into eight segments (of 32 time steps) with transition zones after each segment (of 15 time steps). With this time discretization and for the adopted mesh the computation takes about 40 h of CPU on an IBM Risc 6000 model 39H computer. The equilibrium was obtained at each time step belonging to each of the adopted eight segments by means of an iterative procedure taking into account the unbalanced forces from each time step till the end of the transition zone. The total number of iterations divided by the number of time steps is about 100 (obviously, in each segment, the number of iterations is greater for the initial time steps than for the last). The hard disk storage was approximately 300 MB. So a larger mesh was not adopted, neither a greater time interval for accelerations history, which would allow assuming zero accelerations during the final part of the history. The adopted method considers actions and responses periodic, so that zero final part of accelerations time history would allow the structure to stop by damping effect, before a new period begins. However, even with these approximations, we expect to capture the main aspects of the dam's response on the safe side and obtain a comparison for elastic behaviour with the stochastic stationary hypotheses.

On the other hand, the high damping used covers the fact that in the adopted model there is no dissipation of energy at the joints. Therefore the amplification ratio, about 2.5, of accelerations measured at the dam during the Northridge earthquake was matched. The adopted joint model assumes no slip (when closed) as a consequence of the influence of the shear boxes. When the contraction joints open, the slip allowed depend on the geometry of the shear boxes and so, in order to facilitate the computations, it was assumed no limit on the slip, depending on the reliability of the model on the results obtained. In order to take into account a more realistic joint behaviour, one should adopt the sub-structure scheme, as done by Fenves [7], where the joints and their neighbourhood are discretized in three dimensions. However, the CPU time would be prohibitive for the computer used.

Copyright © 2000 John Wiley & Sons, Ltd

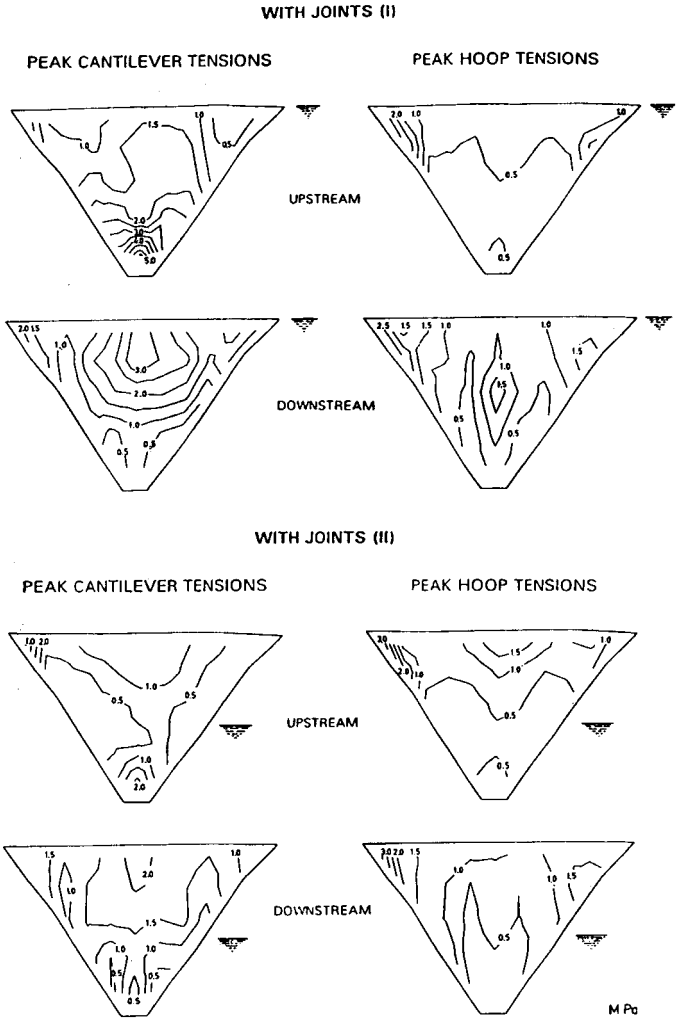

Figure 5. Peak tensile stresses for hypotheses I and II.

As the unbalanced time forces have high-frequency components that originate divergence of the scheme, we must cut off those forces above a certain frequency limit (as a first trial we set this limit at 12 Hz).

From the computed results we conclude that

(i) The hoop compressive peak stresses are higher when no tension contraction joints are taken into account in dam's behaviour.
(ii) For water level at $\frac{1}{3}$ of the dam's height (as occurred during the San Fernando earthquake) no cracking is expected due to the seismic vibrations.

Copyright © 2000 John Wiley & Sons, Ltd

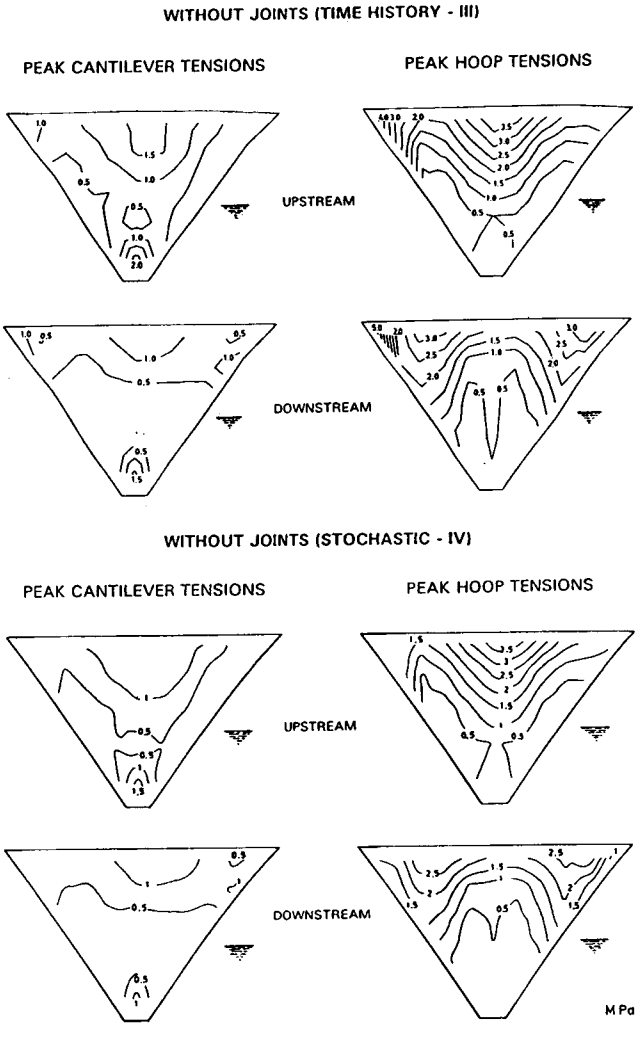

Figure 6. Peak tensile stresses for hypotheses III and IV.

(iii) The average of stresses peak values occurring during consecutive 5 s time intervals (as shown by the stochastic computations for hypothesis IV) it is not much different from the 5 s sample used for hypothesis III. In order to be the same would be necessary to compute the response of the dam to several earthquakes with the same power density and to average the peak values. So the response of the dam to the accelerations time history sample used is representative of earthquakes with similar spectral properties.

(iv) The computed peak accelerations at dam's body including the ratio from the abutments to the top and bottom of central cantilever are about the ratio observed [2] during the 1994 Northridge earthquake.

Copyright © 2000 John Wiley & Sons, Ltd

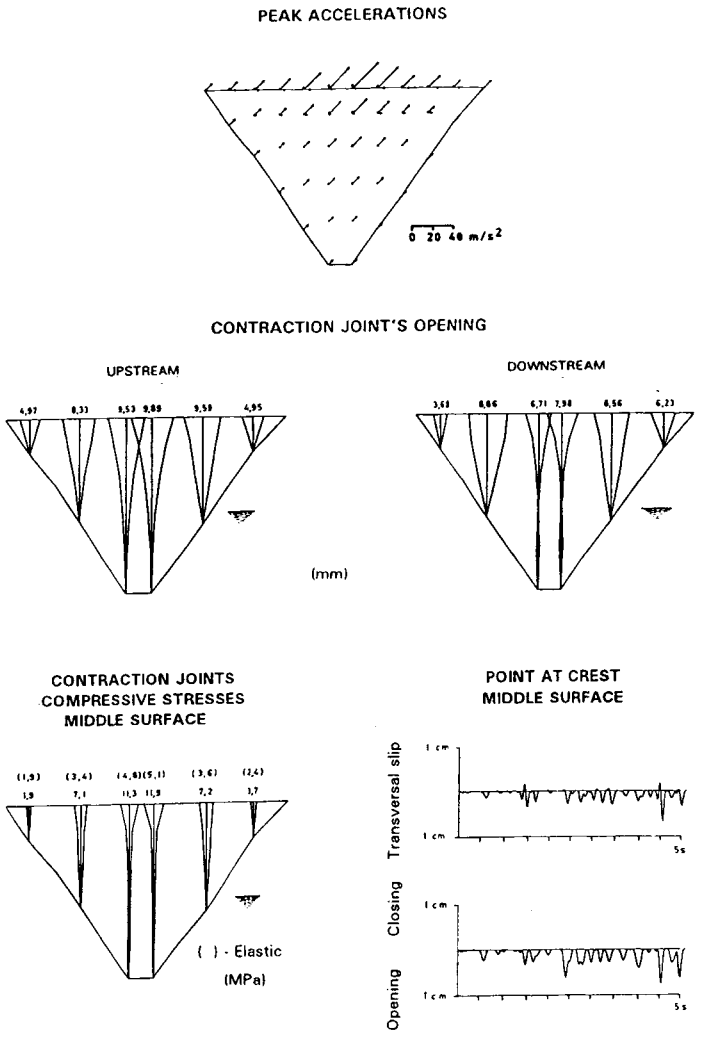

Figure 7. Peak accelerations at dam's body and motions of the joints for hypothesis II.

(v) The computed joint motion is reasonable, as we may conclude from the performance of the prototype during the 1994 Northridge earthquake [8]. We must note the strong impact due to the closure of the contraction joints, yet with peak compressive stresses lower than the expected concrete uniaxial compressive dynamic strength. The joint deformations when closed are assumed elastic and are compatible with the expected joint thickness (about 2 cm thick). The nodal joint compressions (closure times joint rigidity) depend on the correct evaluation of the difference of displacements at local joint axis (must be completely compatible with used joint stiffness hypothesis).

Copyright © 2000 John Wiley & Sons, Ltd

A global equilibrium (referred to nodal forces and moments) was assumed between shell elements (straight cross-sections with linear equivalent stress distributions due to assumed elastic behaviour, without any ruptures) and the joint elements (bilinear stress distribution at cross section characterised by a diagram with zero tensile stresses). Based on simple equilibrium considerations (and on the performance of used finite elements), the compressive hoop stresses computed at joints are more reliable then the hoop stresses computed at shell elements. The computed low values of joint openings may depend both on the number of joints assumed at the dam model and on the coarse mesh adopted and Kirchoff hypothesis of shell elements. In fact, the imposed restrictions on the possible deformed shapes may originate lower radial displacements. The computed high values of compressive hoop stresses may depend on the zero tensile strength hypothesis assumed at contraction joints.

6. CONCLUSION

The adopted method takes into account the influence of the reservoir and foundation, idealised as infinite media. The radiation effect of elastic waves (foundation) and of pressure waves (reservoir) are better modelled than with traditional methods (finite elements with asymptotic radiation boundary conditions) although this aspect is only formal. It also takes into account the spatial variability of the earthquake and the influence of no-tension contraction joints on dam's response. The use of finite element method with time discretization (solving hyperbolic equations) is usually conditioned by the time and space steps necessary to accurately represent the propagation of stress and displacement pulses. The method presented has the accuracy of static finite elements due to the use of harmonic solutions (solving elliptic equations).

The chosen example of Pacoima arch dam under a severe earthquake shows, as expected, that the maximum peak hoop tensions are lower than the ones computed for the hypothesis of neglecting the influence of contraction joints. The maximum peak cantilever tensions obtained when the water is about $\frac{1}{3}$ the dam height would not originate horizontal cracks near the central top zone, as observed during the San Fernando earthquake. According to Sharma [8, 9], the cracking that occurred at the left abutment may be explained by permanent foundation displacements acting as static settlements. The computed compressive stresses at mid-section of the joint elements were lower than the concrete uniaxial dynamic strength.

ACKNOWLEDGEMENTS

The author thanks to the Director of National Laboratory of Civil Engineering for allowing the research work presented, and to the Foundation for Science and Technology for partial financial support of the project. The author also thanks to the reviewers, whose points of view contributed to a substantial improvement of the paper.

REFERENCES

1. Dowling MJ, Hall JF. Non-linear seismic analysis of arch dams. *Journal of Engineering Mechanics, ASCE* 1989; **115**:4.
2. Mojtahedi S, Fenves GL. Response of a concrete arch dam in the 1994 Northridge, California earthquake. *11*th *World Conference on Earthquake Engineering*, Acapulco, 1996.

Copyright © 2000 John Wiley & Sons, Ltd

3. Zhang L, Chopra AK. Computation of spatially varying ground motion and foundation rock impedance matrices for seismic analysis of arch dams. *Report UCB/EERC-91/06*, May 1991.
4. Câmara RC, Coupled arch dam-foundation-reservoir seismic behaviour. Safety evaluation for rupture scenarios, *Ph.D. Thesis*, F.E.U.P., Oporto, 1992. (in Portuguese).
5. Wolf JP, *Soil-Structure-Interaction Analysis in Time Domain*, Prentice-Hall: Englewood Cliffs, NJ: 1988.
6. California Institute of Technology, Strong-motion earthquake accelerograms. Digitised and plotted data. *Report EERL 72-51,* 1973.
7. Fenves GL, Mojtahedi S, Reimer RB. ADAP-88. A computer program for non-linear analysis of concrete arch dams. *Report UCB/EERC-89/12*, Nov. 1989.
8. Sharma RP, Jackson HE, Kumar S. Response of Pacoima dam to the January 17, 1994 Northridge Earthquake, *60th Annual USCOLD Lecture Series, Seismic Design and Performance of Dams,* Los Angeles, 1996.
9. Sharma RP, Jackson HE, Kumar S. Effects of the January 17, 1994 Northridge earthquake on Pacoima arch dam and interim remedial repairs, *19th ICOLD Meeting,* Florence, 1997.

Copyright © 2000 John Wiley & Sons, Ltd